IEEE Access
Multidisciplinary : Rapid Review : Open Access Journal

Received December 6, 2020, accepted December 30, 2020, date of publication January 5, 2021, date of current version January 20, 2021.

Digital Object Identifier 10.1109/ACCESS.2021.3049301

A New Online Learned Interval Type-3 Fuzzy Control System for Solar Energy Management Systems

ZHI LIU[1], ARDASHIR MOHAMMADZADEH[2], HAMZA TURABIEH[3], MAJDI MAFARJA[4], SHAHAB S. BAND[5,6], AND AMIR MOSAVI[7,8,9]

[1]School of Electrical and Automation Engineering, East China Jiaotong University, Nanchang 330013, China
[2]Department of Electrical Engineering, Faculty of Engineering, University of Bonab, Bonab 5551761167, Iran
[3]Department of Information Technology, College of Computers and Information Technology, Taif University, Taif 21944, Saudi Arabia
[4]Department of Computer Science, Birzeit University, Birzeit 627, Palestine
[5]Future Technology Research Center, College of Future, National Yunlin University of Science and Technology, Yunlin 64002, Taiwan
[6]Institute of Research and Development, Duy Tan University, Da Nang 550000, Vietnam
[7]Faculty of Civil Engineering, Technische Universität Dresden, 01069 Dresden, Germany
[8]School of Economics and Business, Norwegian University of Life Sciences, 1430 Ås, Norway
[9]John von Neumann Faculty of Informatics, Obuda University, 1034 Budapest, Hungary

Corresponding authors: Shahab S. Band (shamshirbands@yuntech.edu.tw) and Amir Mosavi (amir.mosavi@mailbox.tu-dresden.de)

This work was supported by Open Access Funding by the Publication Fund of the TU Dresden. The work of Hamza Turabieh was supported by the Taif University, Taif, Saudi Arabia, under Project TURSP-2020/125.

ABSTRACT In this article, a novel method based on interval type-3 fuzzy logic systems (IT3-FLSs) and an online learning approach is designed for power control and battery charge planing for photovoltaic (PV)/battery hybrid systems. Unlike the other methods, the dynamics of battery, PV and boost converters are considered to be fully unknown. Also, the effects of variation of temperature, radiation, and output load are taken into account. The robustness and the asymptotic stability of the proposed method is analyzed by the Lyapunov/LaSalle's invariant set theorems, and the tuning rules are extracted for IT3-FLS. Also, the upper bound of approximation error (AE) is approximated, and then a new compensator is designed to deal with the effects of dynamic AEs. The superiority of the proposed method is examined in several conditions and is compared with some other well-known methods. It is shown that the schemed method results in high performance under difficult conditions such as variation of temperature and radiation and abruptly changing in the output load.

INDEX TERMS Fuzzy systems, learning algorithms, power management, type-3 fuzzy systems, adaptive control, machine learning, artificial intelligence.

I. INTRODUCTION

Energy management is one of the hot topics in recent years. Especially, solar energies and storage systems increasingly attract attention. Solar energy has some features which have caused studies in this field to be attractive. The sun is one of the most abundant energy sources that do not pollute the environment [1]–[3]. Using solar energy can directly affect on the reduction of carbon footprint on the earth and the changing of future climate. The maintenance cost of photovoltaic (PV) panels is also remarkable less. However, the main drawback is the high dependence of solar energy on weather conditions. Then it is vital that the energy storage systems and energy management methods to be developed such that the maximum power to be extracted and the output load voltage to be regulated on the reference level. The basic approach is the use of boost converters to make a switching mechanism between energy storage systems and PV panels [4], [5].

Recently, several control methods have been developed to manage switching frequency such that the maximum power to be extracted and the voltage to be kept on a reference level in verses of load changes, the variation of temperature and time-varying radiation. For instance, in [6], an optimal charging plan is designed for battery, and energy consumption in peak times is investigated. In [7], considering electrical power cost, a predictive control system is presented for energy control in the photovoltaic systems. In [8], by the use of a gravitational search technique, a controller is designed

The associate editor coordinating the review of this manuscript and approving it for publication was Jenny Mahoney.

for power management and for optimal battery charging. In [9], a passivity-based control system is proposed, and the effect of variation of load resistance is studied. In [10], the frequency stability in a PV/battery/hydropower microgrid is investigated by the use of a small-signal state-space model to guarantee the desired power-sharing. In [11], an energy balance system is presented by the current control approach, and the power-sharing between various units is studied. In [12], by weather forecasting technique, the level of radiation is predicted, and a battery charging pattern is designed. In [13], the problem of battery overcharging and deep discharge is studied by designing a supervision unit. In [14], by the use of DC-DC converters and optimal control systems, the problem of maximum power extracting is studied. In [15], the battery charge balancing is studied by the use of a sliding mode controller and its performance is examined considering the European benchmark microgrid. In [16], a risk management technique is proposed to generate a balanced hybrid energy system such that the market price uncertainty is taken to account.

One of the drawbacks of the reviewed energy management systems is that the parameter and dynamic uncertainty and uncertain weather conditions are not handled, effectively. To cope with uncertain dynamics and parameters some fuzzy logic system (FLS) based approaches have been introduced [17]–[19]. For instance, in [20], a FLS based algorithm is developed to guarantee the voltage stability in the PV/battery system and the battery charging and discharging strategy is studied. Similar to [20], in [21], an FLS based controller is presented for the energy storage system such that the stability of the PV system to be ensured. A fractionala-order FLS controller is suggested in [22], for power/voltage control. In [23], a supervisor system is designed by the use of FLSs to construct a power balance between various energy generators such as wind, PV, and diesel systems. In [24], to guarantee the power availability, an FLS is designed and its effectiveness is examined through a case study considering Morocco city. In [25], considering electricity price and pollutant treatment cost, a FLS based control system is designed to control the battery system. In [26], a new algorithm is suggested using FLSs to stabilize the output voltage and extract maximum power in PV. In [27], charging/discharging plans of battery systems using FLS are studied and the performance of the suggested method is examined on multi-type of batteries. In [28], the gains of the PI controller is optimized using FLSs to extract optimal power in the PV/battery system and the effectiveness of the FLS is shown by comparison with the conventional P&O method. The well efficiency of neural-fuzzy based controllers have been shown in other control problems such as Markov jump and descriptor systems, networked systems, nontriangular systems, multiagent systems and observer systems [29]–[34].

The main disadvantages of the above reviewed fuzzy based controllers for PV/battery system are that (1) simple FLSs are used to cope with uncertainties, (2) the effects of time-varying dynamics and radiations are not taken to account, (3) the stability and robustness of FLS based controller are not studied and (4) the learning algorithms with complicated structure and computational cost are used. Recently improved type-2 FLS (T2-FLS) and IT3-FLS have been presented [35]–[37]. It has been shown that improved FLSs result in higher performance in the wide engineering applications such as: model identification [38], fault detection problems [39], robotic systems [40], medical diagnosis systems [41], forecasting problems [42], control systems [38], classification problems [43], image processing [44], decision-making systems [45], and so on. Regarding above motivation, in current study a new FLS based controller using IT3-FLSs is proposed for planing a charge/discharge storage system and an output voltage regulator. The stability and robustness are studied and various challenging conditions are considered, such as variation of temperature, time-varying radiation, and unknown dynamics of PV/battery system. The main contributions are:

- The effects of variation of temperature, abruptly changes in output load and time-varying radiation are taken into account and the uncertainties are estimated by IT3-FLSs.
- The optimization of IT3-FLSs and control signals are carry out by Lyapunov and LaSall's theorems.
- The upper bound of AE is approximated and a compensator is designed to cope with the effect of AEs.
- The dynamics of all units such as battery, PV and convertors are considered to be fully unknown and the effects of dynamic estimation errors are eliminated by the suggested compensators.

II. PROBLEM DESCRIPTION

A. GENERAL INVESTIGATION

The block diagrams of the main hybrid system and control system are depicted in Figs. 1-2. As it is seen, the system includes PV, battery, boost convertor and bidirectional boost convertor. The control objective is the planing of an appropriate charge/discharge plan for battery and an appropriate current for PV to regulate the load voltage in a desired level. In the following, the mathematical dynamics of all units are illustrated.

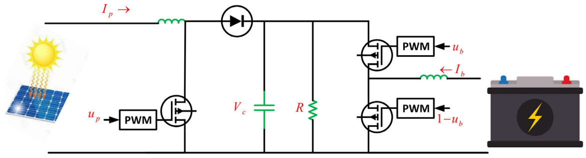

FIGURE 1. The block diagram of PV/battery hybrid plant.

B. CONVERTERS

The Boost and bidirectional Boost convertors construct the switching unit. The task of these units is to make a switching mechanism between battery and PV. The model of switching unit in the form of state space is written by taking average of

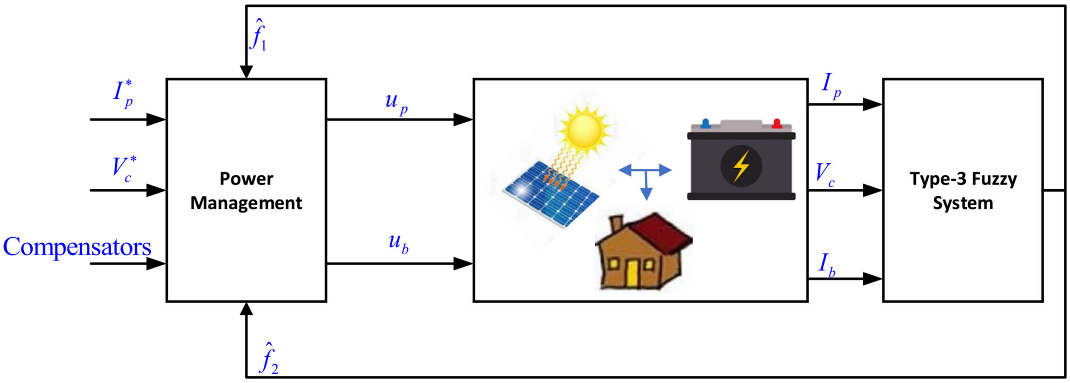

FIGURE 2. The suggested control system.

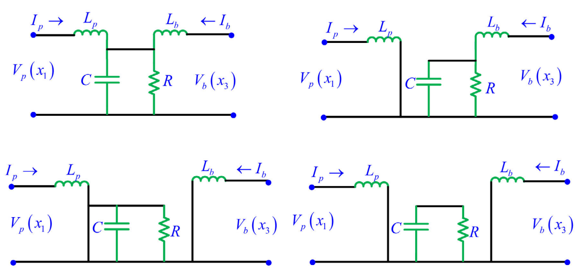

FIGURE 3. Switching circuit modes.

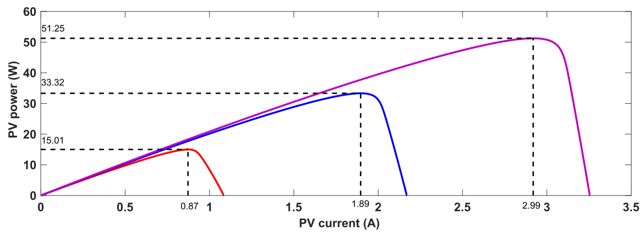

FIGURE 4. The power of the PV panel as a function of its current.

four modes (see Fig. 3):

$$\dot{y}_1 = \frac{1}{L_p}\left(-y_2 + y_2 u_p + V_p(y_1)\right)$$
$$\dot{y}_2 = \frac{1}{C}\left(y_1 - y_1 u_p - y_2/R + y_3 u_b\right)$$
$$\dot{y}_3 = \frac{1}{L_b}\left(-y_2 u_b + V_b(y_3)\right) \quad (1)$$

where, I_p and I_b are the currents of PV and battery respectively and V_c is the load voltage.

C. PV MODELING

The important approach to model behaviour of PV panel that is frequently reported in many studies is the single-diode approach: [46]

$$i_{ph} = s\left(k_i\left(T - T_r\right) + i_{sc}\right)$$
$$I_p = -i_o \exp\left(\frac{q}{nTk_b}\left(V_p + I_p R_{sg}\right) - 1\right) + GI_{phg} - \left(I_p R_{sg} + V_p\right)/R_{shg}$$
$$i_0 = \exp\left[\frac{E_g q}{k_b A}\left(\frac{1}{T_r + 273} - \frac{1}{T + 273}\right)\right]\left(\frac{T + 273}{T_r + 273}\right)^3 i_r \quad (2)$$

where the parameters description is given in Table 1. The power of PV as a function of its current is given in Fig. 4. As it is observed, the maximum power is obtained in one special current. The controller should adjust the current of PV at this special level.

D. BATTERY MODELING

The mathematical equations of battery is written as [46]:

$$E(t) = -\int W_{Loss} + \beta I_b V_{boc} dt, \quad V_b = V_{boc} - r_b I_b$$
$$\beta = \begin{cases} \beta_1 & I_b \geq 0 \\ \beta_2 & I_b < 0, \end{cases} \quad SoC(t) = E(t)/E_{Max} \quad (3)$$

where, the parameter descriptions are given in Table 2.

III. PROPOSED TYPE-3 FLS

The interval type-3 FLSs (IT3-FLSs) are developed to handle more level of uncertainties [37]. In this study, IT3-FLSs are used for online dynamic identification. The structure of IT3-FLS (see Fig. 5) is explained step-by-step in below:

1) The inputs of IT3-FLSs are $y_1 = I_p(t)$, $y_2 = V_c(t - \tau)$, $y_3 = I_b(t)$, where, I_p and I_b are the currents of PV and battery, respectively and V_c is the load voltage. τ represents the sample time.

2) For each input, two Gaussian membership functions (MFs) (see Fig. 6) are considered. The centers of MFs are

TABLE 1. Description the parameters of PV model.

Parameter	Description
n	Number of cells
$G\left(w/m^2\right)$	Solar radiation
$k_b\,(J/K)$	Boltzmann's constant
R_{sh} and $R_s\,(\Omega)$	Equivalent resistances
$T\,(^\circ c)$	Temperature of PV
q	Electron charge
A	Constant of the diode ideality
$E_g\,(ev)$	Energy of Band-Gap
$i_r\,(A)$	Saturation current
$i_{ph}\,(A)$	Photo generated currents
$T_r\,(^\circ c)$	Reference temperature

TABLE 2. Description the parameters of battery model.

Parameter	Description
$r_b\,(\Omega)$	Internal resistance
$E_{\mathrm{Max}}\,(J)$	Maximum savable energy
$V_{boc}\,(v)$	Open circuit Voltage
$W_{Loss}\,(w)$	Power losses
β_1 and β_2	Charge/Discharge rates

set to the upper and lower bounds of each input. For input I_p, the upper and lower memberships are obtained as:

$$\bar{\mu}_{\tilde{A}^1_{I_p}|\alpha}\left(I_p\right) = \exp\left(-\frac{\left(I_p - \underline{c}_{\tilde{A}^1_{I_p}}\right)^2}{\bar{\sigma}^2_{\tilde{A}^1_{I_p}|\alpha}}\right)$$
$$\bar{\mu}_{\tilde{A}^2_{I_p}|\alpha}\left(I_p\right) = \exp\left(-\frac{\left(I_p - \bar{c}_{\tilde{A}^2_{I_p}}\right)^2}{\bar{\sigma}^2_{\tilde{A}^2_{I_p}|\alpha}}\right) \tag{4}$$
$$\underline{\mu}_{\tilde{A}^1_{I_p}|\alpha}\left(I_p\right) = \exp\left(-\frac{\left(I_p - \underline{c}_{\tilde{A}^1_{I_p}}\right)^2}{\underline{\sigma}^2_{\tilde{A}^1_{I_p}|\alpha}}\right)$$
$$\underline{\mu}_{\tilde{A}^2_{I_p}|\alpha}\left(I_p\right) = \exp\left(-\frac{\left(I_p - \bar{c}_{\tilde{A}^2_{I_p}}\right)^2}{\underline{\sigma}^2_{\tilde{A}^2_{I_p}|\alpha}}\right) \tag{5}$$

where, α is level of the horizontal slice. $\tilde{A}^1_{I_p}$ and $\tilde{A}^2_{I_p}$ are the first and second MFs for input I_p. $\underline{c}_{\tilde{A}^1_{I_p}}$ and $\bar{c}_{\tilde{A}^2_{I_p}}$ are the centers of $\tilde{A}^1_{I_p}$ and $\tilde{A}^2_{I_p}$, respectively. $\bar{\sigma}_{\tilde{A}^1_{I_p}|\alpha}/\underline{\sigma}_{\tilde{A}^1_{I_p}|\alpha}$ and $\bar{\sigma}_{\tilde{A}^2_{I_p}|\alpha}/\underline{\sigma}_{\tilde{A}^2_{I_p}|\alpha}$ are the standard division for the upper/lower bounds of $\tilde{A}^1_{I_p}$ and $\tilde{A}^2_{I_p}$, respectively. Similarly, for input I_b, one has:

$$\bar{\mu}_{\tilde{A}^1_{I_b}|\alpha}\left(I_b\right) = \exp\left(-\frac{\left(I_b - \underline{c}_{\tilde{A}^1_{I_b}}\right)^2}{\bar{\sigma}^2_{\tilde{A}^1_{I_b}|\alpha}}\right)$$
$$\bar{\mu}_{\tilde{A}^2_{I_b}|\alpha}\left(I_b\right) = \exp\left(-\frac{\left(I_b - \bar{c}_{\tilde{A}^2_{I_b}}\right)^2}{\bar{\sigma}^2_{\tilde{A}^2_{I_b}|\alpha}}\right) \tag{6}$$
$$\underline{\mu}_{\tilde{A}^1_{I_b}|\alpha}\left(I_b\right) = \exp\left(-\frac{\left(I_b - \underline{c}_{\tilde{A}^1_{I_b}}\right)^2}{\underline{\sigma}^2_{\tilde{A}^1_{I_b}|\alpha}}\right)$$
$$\underline{\mu}_{\tilde{A}^2_{I_b}|\alpha}\left(I_b\right) = \exp\left(-\frac{\left(I_b - \bar{c}_{\tilde{A}^2_{I_b}}\right)^2}{\underline{\sigma}^2_{\tilde{A}^2_{I_b}|\alpha}}\right) \tag{7}$$

where, $\tilde{A}^1_{I_b}$ and $\tilde{A}^2_{I_b}$ are the first and second MFs for input I_b. $\underline{c}_{\tilde{A}^1_{I_b}}$ and $\bar{c}_{\tilde{A}^2_{I_b}}$ are the centers of $\tilde{A}^1_{I_b}$ and $\tilde{A}^2_{I_b}$, respectively. $\bar{\sigma}_{\tilde{A}^1_{I_b}|\alpha}/\underline{\sigma}_{\tilde{A}^1_{I_b}|\alpha}$ and $\bar{\sigma}_{\tilde{A}^2_{I_b}|\alpha}/\underline{\sigma}_{\tilde{A}^2_{I_b}|\alpha}$ are the standard division for the upper/lower bounds of $\tilde{A}^1_{I_b}$ and $\tilde{A}^2_{I_b}$, respectively. Finally, for input V_c, one has:

$$\bar{\mu}_{\tilde{A}^1_{V_c}|\alpha}\left(V_c\right) = \exp\left(-\frac{\left(V_c - \underline{c}_{\tilde{A}^1_{V_c}}\right)^2}{\bar{\sigma}^2_{\tilde{A}^1_{V_c}|\alpha}}\right)$$

$$\bar{\mu}_{\tilde{A}^2_{V_c}|\alpha}(V_c) = \exp\left(-\frac{\left(V_c - \bar{c}_{\tilde{A}^2_{V_c}}\right)^2}{\bar{\sigma}^2_{\tilde{A}^2_{V_c}|\alpha}}\right) \tag{8}$$

$$\underline{\mu}_{\tilde{A}^1_{V_c}|\alpha}(V_c) = \exp\left(-\frac{\left(V_c - \underline{c}_{\tilde{A}^1_{V_c}}\right)^2}{\underline{\sigma}^2_{\tilde{A}^1_{V_c}|\alpha}}\right)$$

$$\underline{\mu}_{\tilde{A}^2_{V_c}|\alpha}(V_c) = \exp\left(-\frac{\left(V_c - \bar{c}_{\tilde{A}^2_{V_c}}\right)^2}{\underline{\sigma}^2_{\tilde{A}^2_{V_c}|\alpha}}\right) \tag{9}$$

where, $\tilde{A}^1_{V_c}$ and $\tilde{A}^2_{V_c}$ are the first and second MFs for input V_c. $\underline{c}_{\tilde{A}^1_{V_c}}$ and $\bar{c}_{\tilde{A}^2_{V_c}}$ are the centers of $\tilde{A}^1_{V_c}$ and $\tilde{A}^2_{V_c}$, respectively. $\bar{\sigma}_{\tilde{A}^1_{V_c}|\alpha}/\underline{\sigma}_{\tilde{A}^1_{V_c}|\alpha}$ and $\bar{\sigma}_{\tilde{A}^2_{V_c}|\alpha}/\underline{\sigma}_{\tilde{A}^2_{V_c}|\alpha}$ are the standard division for the upper/lower bounds of $\tilde{A}^1_{V_c}$ and $\tilde{A}^2_{V_c}$, respectively. 3) The output of $\hat{f}_1$ and $\hat{f}_2$ are:

$$\begin{aligned}\hat{f}_1 &= \theta_1^T \zeta_1\\ \hat{f}_2 &= \theta_2^T \zeta_2\end{aligned} \tag{10}$$

where, θ_i and ζ_i are:

$$\begin{aligned}\theta_i &= \left[\underline{w}_{i1}, \ldots, \underline{w}_{iR}, \bar{w}_{i1}, \ldots, \bar{w}_{iR}\right]^T\\ \zeta_i &= \left[\underline{\zeta}_{i1}, \ldots, \underline{\zeta}_{iR}, \bar{\zeta}_{i1}, \ldots, \bar{\zeta}_{iR}\right]^T\end{aligned} \tag{11}$$

where, $\bar{w}_{il}$ and $\underline{w}_{il}$ are the parameters of $l-th$ rule for $i-th$ IT3-FLS and R represents the number of rules. $\underline{\zeta}_{il}$ and $\bar{\zeta}_{il}$ are:

$$\bar{\zeta}_l = \frac{\sum_{j=1}^{n_\alpha} \bar{\alpha}_j \frac{\bar{z}^l_{\mu_s=\bar{\alpha}_j}}{\sum_{l=1}^{R}\left(\bar{z}^l_{\mu_s=\bar{\alpha}_j}+\underline{z}^l_{\mu_s=\bar{\alpha}_j}\right)}}{\sum_{j=1}^{n_\alpha}\left(\bar{\alpha}_j + \underline{\alpha}_j\right)} + \frac{\sum_{j=1}^{n_\alpha} \underline{\alpha}_j \frac{\bar{z}^l_{\mu_s=\underline{\alpha}_j}}{\sum_{l=1}^{R}\left(\bar{z}^l_{\mu_s=\underline{\alpha}_j}+\underline{z}^l_{\mu_s=\underline{\alpha}_j}\right)}}{\sum_{j=1}^{n_\alpha}\left(\bar{\alpha}_j + \underline{\alpha}_j\right)}, \quad l = 1, \ldots, 8 \tag{12}$$

$$\underline{\zeta}_l = \frac{\sum_{j=1}^{n_\alpha} \bar{\alpha}_j \frac{\underline{z}^l_{\mu_s=\bar{\alpha}_j}}{\sum_{l=1}^{R}\left(\bar{z}^l_{\mu_s=\bar{\alpha}_j}+\underline{z}^l_{\mu_s=\bar{\alpha}_j}\right)}}{\sum_{j=1}^{n_\alpha}\left(\bar{\alpha}_j + \underline{\alpha}_j\right)} + \frac{\sum_{j=1}^{n_\alpha} \underline{\alpha}_j \frac{\underline{z}^l_{\mu_s=\underline{\alpha}_j}}{\sum_{l=1}^{R}\left(\bar{z}^l_{\mu_s=\underline{\alpha}_j}+\underline{z}^l_{\mu_s=\underline{\alpha}_j}\right)}}{\sum_{j=1}^{n_\alpha}\left(\bar{\alpha}_j + \underline{\alpha}_j\right)}, \quad l = 1, \ldots, 8 \tag{13}$$

where, n_α is the number of horizontal slices and:

$$\underline{\zeta}_l = \frac{\sum_{j=1}^{n_\alpha} \bar{\alpha}_j \frac{\underline{z}^l_{\mu_s=\bar{\alpha}_j}}{\sum_{l=1}^{R}\left(\bar{z}^l_{\mu_s=\bar{\alpha}_j}+\underline{z}^l_{\mu_s=\bar{\alpha}_j}\right)}}{\sum_{j=1}^{n_\alpha}\left(\bar{\alpha}_j + \underline{\alpha}_j\right)} + \frac{\sum_{j=1}^{n_\alpha} \underline{\alpha}_j \frac{\underline{z}^l_{\mu_s=\underline{\alpha}_j}}{\sum_{l=1}^{R}\left(\bar{z}^l_{\mu_s=\underline{\alpha}_j}+\underline{z}^l_{\mu_s=\underline{\alpha}_j}\right)}}{\sum_{j=1}^{n_\alpha}\left(\bar{\alpha}_j + \underline{\alpha}_j\right)}, \quad l = 1, \ldots, R \tag{14}$$

$$\begin{aligned}
\underline{z}_{\mu_s} &= \bar{\alpha}^l_j = \underline{\mu}_{\tilde{A}^{k_{I_p}}_{I_p}|\bar{\alpha}_j}(I_p)\, \underline{\mu}_{\tilde{A}^{k_{I_b}}_{I_b}|\bar{\alpha}_j}(I_b)\, \underline{\mu}_{\tilde{A}^{k_{V_c}}_{V_c}|\bar{\alpha}_j}(V_c)\\
\underline{z}_{\mu_s} &= \underline{\alpha}_j{}^l = \underline{\mu}_{\tilde{A}^{k_{I_p}}_{I_p}|\underline{\alpha}_j}(I_p)\, \underline{\mu}_{\tilde{A}^{k_{I_b}}_{I_b}|\underline{\alpha}_j}(I_b)\, \underline{\mu}_{\tilde{A}^{k_{V_c}}_{V_c}|\underline{\alpha}_j}(V_c)\\
\bar{z}_{\mu_s} &= = \bar{\alpha}_j{}^l = \bar{\mu}_{\tilde{A}^{k_{I_p}}_{I_p}|\bar{\alpha}_j}(I_p)\, \bar{\mu}_{\tilde{A}^{k_{I_b}}_{I_b}|\bar{\alpha}_j}(I_b)\, \bar{\mu}_{\tilde{A}^{k_{V_c}}_{V_c}|\bar{\alpha}_j}(V_c)\\
\bar{z}_{\mu_s} &= \underline{\alpha}_j{}^l = \bar{\mu}_{\tilde{A}^{k_{I_p}}_{I_p}|\underline{\alpha}_j}(I_p)\, \bar{\mu}_{\tilde{A}^{k_{I_b}}_{I_b}|\underline{\alpha}_j}(I_b)\, \bar{\mu}_{\tilde{A}^{k_{V_c}}_{V_c}|\underline{\alpha}_j}(V_c)
\end{aligned} \tag{15}$$

where, $k_{I_p} = 1, 2$, $k_{I_b} = 1, 2$ and $k_{V_c} = 1, 2$. The rules are written as:

$$\begin{aligned}
&\text{Rule \#1}: \text{If } I_p \text{ is } \tilde{A}^1_{I_p}|\alpha \text{ and } I_b \text{ is } \tilde{A}^1_{I_b}|\alpha \text{ and } V_c \text{ is } \tilde{A}^1_{V_c}|\alpha\\
&\qquad \text{Then } \hat{f}_i \in \left[\underline{w}_{i1}, \bar{w}_{i1}\right]\\
&\text{Rule \#2}: \text{If } I_p \text{ is } \tilde{A}^1_{I_p}|\alpha \text{ and } I_b \text{ is } \tilde{A}^1_{I_b}|\alpha \text{ and } V_c \text{ is } \tilde{A}^2_{V_c}|\alpha\\
&\qquad \text{Then } \hat{f}_i \in \left[\underline{w}_{i2}, \bar{w}_{i2}\right]\\
&\text{Rule \#3}: \text{If } I_p \text{ is } \tilde{A}^1_{I_p}|\alpha \text{ and } I_b \text{ is } \tilde{A}^2_{I_b}|\alpha \text{ and } V_c \text{ is } \tilde{A}^1_{V_c}|\alpha\\
&\qquad \text{Then } \hat{f}_i \in \left[\underline{w}_{i3}, \bar{w}_{i3}\right]\\
&\text{Rule \#4}: \text{If } I_p \text{ is } \tilde{A}^1_{I_p}|\alpha \text{ and } I_b \text{ is } \tilde{A}^2_{I_b}|\alpha \text{ and } V_c \text{ is } \tilde{A}^2_{V_c}|\alpha\\
&\qquad \text{Then } \hat{f}_i \in \left[\underline{w}_{i4}, \bar{w}_{i4}\right]\\
&\text{Rule \#5}: \text{If } I_p \text{ is } \tilde{A}^2_{I_p}|\alpha \text{ and } I_b \text{ is } \tilde{A}^1_{I_b}|\alpha \text{ and } V_c \text{ is } \tilde{A}^1_{V_c}|\alpha\\
&\qquad \text{Then } \hat{f}_i \in \left[\underline{w}_{i5}, \bar{w}_{i5}\right]\\
&\text{Rule \#6}: \text{If } I_p \text{ is } \tilde{A}^2_{I_p}|\alpha \text{ and } I_b \text{ is } \tilde{A}^1_{I_b}|\alpha \text{ and } V_c \text{ is } \tilde{A}^2_{V_c}|\alpha\\
&\qquad \text{Then } \hat{f}_i \in \left[\underline{w}_{i6}, \bar{w}_{i6}\right]\\
&\text{Rule \#7}: \text{If } I_p \text{ is } \tilde{A}^2_{I_p}|\alpha \text{ and } I_b \text{ is } \tilde{A}^2_{I_b}|\alpha \text{ and } V_c \text{ is } \tilde{A}^1_{V_c}|\alpha\\
&\qquad \text{Then } \hat{f}_i \in \left[\underline{w}_{i7}, \bar{w}_{i7}\right]\\
&\text{Rule \#8}: \text{If } I_p \text{ is } \tilde{A}^2_{I_p}|\alpha \text{ and } I_b \text{ is } \tilde{A}^2_{I_b}|\alpha \text{ and } V_c \text{ is } \tilde{A}^2_{V_c}|\alpha\\
&\qquad \text{Then } \hat{f}_i \in \left[\underline{w}_{i8}, \bar{w}_{i8}\right]
\end{aligned} \tag{16}$$

Remark 1: Fig. 6 shows that, in the type-3 MFs, the secondary membership is not a crisp value but it is a fuzzy set. Also a horizontal slice a level $\mu_s = \alpha_k$ is equal with two slices at levels $\mu_s = \underline{\alpha}_k$ and $\mu_s = \bar{\alpha}_k$ in type-2 counterpart.

IV. POWER MANAGEMENT AND STABILITY ANALYSIS

In this section the controllers u_p/u_b are formulated. The main results are summarized in below.

Theorem 1: The closed-loop system is asymptotically stable if control signals and compensators are designed

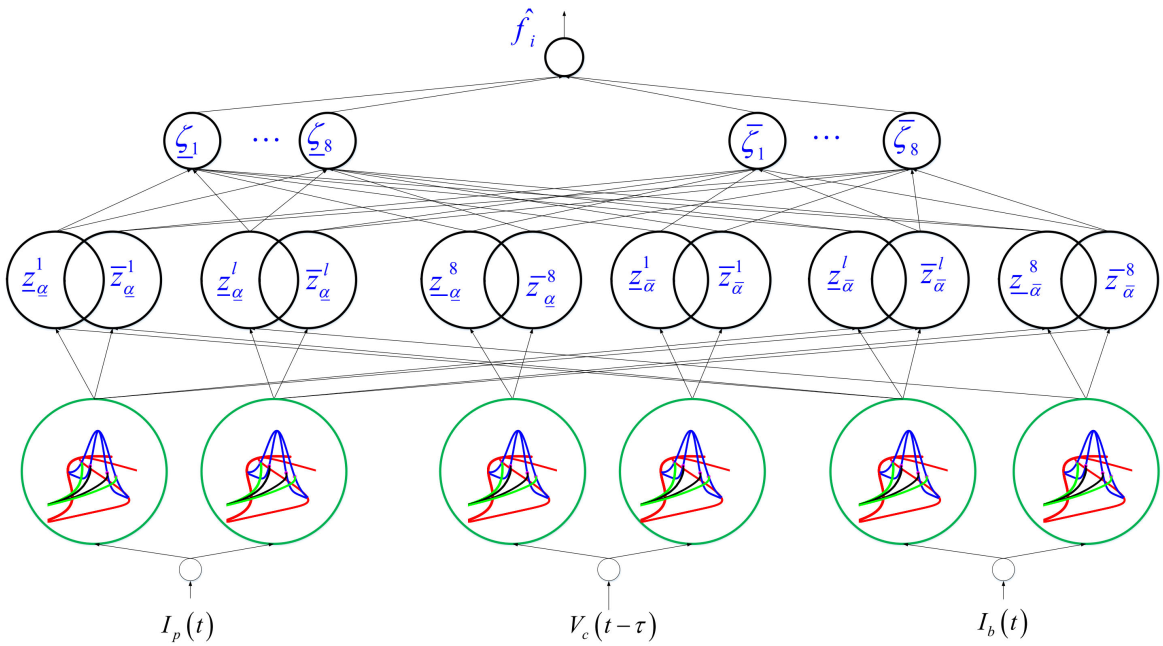

FIGURE 5. The structure scheme of the IT3-FLS.

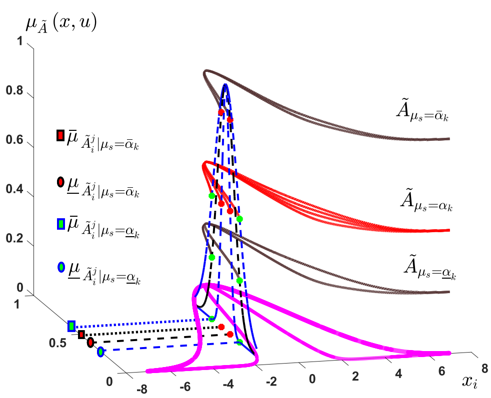

FIGURE 6. The interval type-3 membership function [37].

as (17-18) and tuning rules for parameters of IT3-FLSs and estimated upper bound of approximation error (AE) are considered as (19-20).

$$\begin{aligned} u_p &= \left(-\hat{f}_1(y,\theta_1) - \lambda_1 e_1 + s_{p_c}\right)/\hat{b}_1 \\ u_b &= \left(-\hat{f}_2(y,\theta_2) - \lambda_2 e_2 + s_{b_c}\right)/\hat{b}_2 \end{aligned} \tag{17}$$

$$\begin{aligned} s_{p_c} &= -\hat{\bar{E}}_1 |\tilde{y}_1| \frac{e_1}{|e_1^2| + \varepsilon} \\ s_{b_c} &= -\hat{\bar{E}}_2 |\tilde{y}_2| \frac{e_2}{|e_2^2| + \varepsilon} \end{aligned} \tag{18}$$

$$\begin{aligned} \dot{\hat{\theta}}_1 &= \gamma \tilde{y}_1 \xi_1, \quad \dot{\hat{\theta}}_2 = \gamma \tilde{y}_2 \xi_2 \\ \dot{\hat{b}}_1 &= \gamma \tilde{y}_1 u_p, \ \dot{\hat{b}}_2 = \gamma \tilde{y}_2 u_b \end{aligned} \tag{19}$$

$$\begin{aligned} \dot{\hat{\bar{E}}}_1 &= \gamma |\tilde{y}_1| \\ \dot{\hat{\bar{E}}}_2 &= \gamma |\tilde{y}_2| \end{aligned} \tag{20}$$

where, s_{p_c} and s_{b_c} are compensators, $\lambda_i, \ i = 1, 2$ are positive constants, and $e_1 = \hat{y}_1 - y_{1d}$ and $e_2 = \hat{y}_2 - y_{2d}$ are the tracking errors and y_{1d} and y_{2d} are the optimal signals, γ is adaptation rate, $\hat{f}_i(y, \theta_i, \ i = 1, 2)$ are IT3-FLSs, $\lambda_i, \ i = 1, 2$ are positive constants, $\bar{E}_i, \ i = 1, 2$ are above bound of AE, $\hat{\bar{E}}_1$ and $\hat{\bar{E}}_2$ are estimated upper bound of AE and ε is a small constant.

Proof: The dynamics of y_1 and y_2 in (1) are rewritten as follows:

$$\begin{aligned} \dot{y}_1 &= \frac{1}{L_p}\left(-y_2 + V_p(y_1)\right) + \frac{y_2}{L_p} u_p \\ \dot{y}_2 &= \frac{1}{C}\left(y_1 - y_1 u_p - y_2/R\right) + \frac{y_3}{C} u_b \end{aligned} \tag{21}$$

To design u_p and u_b, one can has:

$$\begin{aligned} \dot{\hat{y}}_1 &= \hat{f}_1(y,\theta_1) + \hat{b}_1 u_p \\ \dot{\hat{y}}_2 &= \hat{f}_2(y,\theta_2) + \hat{b}_2 u_b, \end{aligned} \tag{22}$$

where $\hat{y}_1$, $\hat{y}_2$, $\hat{b}_1$ and $\hat{b}_2$ are the estimation of y_1, y_2, y_2/L_p and y_3/C, respectively and $\hat{f}_1$ and $\hat{f}_2$ are the IT3-FLSs. The structure and parameters of IT3-FLSs $\hat{f}_1$ and $\hat{f}_2$ are illustrated in the previous section. From (21) and (22), the dynamics of $\tilde{y}_1 = y_1 - \hat{y}_1$ and $\tilde{y}_2 = y_2 - \hat{y}_2$ are:

$$\begin{aligned} \dot{\tilde{y}}_1 &= \frac{1}{L_p}\left(-y_2 + V_p(y_1)\right) - \hat{f}_1(y,\theta_1) \\ &\quad + \left(\frac{y_2}{L_p} - \hat{b}_1\right) u_p \\ \dot{\tilde{y}}_2 &= \frac{1}{C}\left(y_1 - y_1 u_p - y_2/R\right) - \hat{f}_2(y,\theta_2) \\ &\quad + \left(\frac{y_3}{C} - \hat{b}_2\right) u_b \end{aligned} \tag{23}$$

From (23), one has:

$$\begin{aligned}\dot{\tilde{y}}_1 &= \hat{f}_1^*\left(y,\theta_1^*\right) - \hat{f}_1\left(y,\theta_1\right) + \left(\hat{b}_1^* - \hat{b}_1\right)u_p \\ &\quad + \frac{1}{L_p}\left(-y_2 + V_p\left(y_1\right)\right)_1 - \hat{f}_1^*\left(y,\theta_1^*\right) + \left(\frac{y_2}{L_p} - \hat{b}_1^*\right)u_p \\ \dot{\tilde{y}}_2 &= \hat{f}_2^*\left(y,\theta_2^*\right) - \hat{f}_2\left(y,\theta_2\right) + \left(\hat{b}_2^* - \hat{b}_2\right)u_b \\ &\quad + \frac{1}{C}\left(y_1 - y_1u_p - y_2/R\right) - \hat{f}_2^*\left(y,\theta_2^*\right) + \left(\frac{y_3}{C} - \hat{b}_2^*\right)u_b\end{aligned} \tag{24}$$

where, $\hat{f}_1^*\left(y,\theta_1^*\right)$ and $\hat{f}_2^*\left(y,\theta_2^*\right)$ are optimal IT3-FLS and $\hat{b}_1^*$ and $\hat{b}_2^*$ are optimal gains. From (24), consider the following definitions:

$$\begin{aligned}E_1 &= \frac{1}{L_p}\left(-y_2 + V_p\left(y_1\right)\right)_1 - \hat{f}_1^*\left(y,\theta_1^*\right) + \left(\frac{y_2}{L_p} - \hat{b}_1^*\right)u_p \\ E_2 &= \frac{1}{C}\left(y_1 - y_1u_p - y_2/R\right) - \hat{f}_2^*\left(y,\theta_2^*\right) + \left(\frac{y_3}{C} - \hat{b}_2^*\right)u_b\end{aligned} \tag{25}$$

From equations (24)-(25), it is concluded that:

$$\begin{aligned}\dot{\tilde{y}}_1 &= E_1 + \tilde{\theta}_1^T\xi_1 + \tilde{b}_1u_p \\ \dot{\tilde{y}}_2 &= E_2 + \tilde{\theta}_2^T\xi_2 + \tilde{b}_2u_b\end{aligned} \tag{26}$$

where ξ_1 and ξ_2 are defined in (12-13) and the variables $\tilde{\theta}$ and $\tilde{b}$ and are described as:

$$\begin{aligned}\tilde{\theta}_1 &= \hat{\theta}_1^* - \hat{\theta}_1,\ \ \tilde{\theta}_2 = \hat{\theta}_2^* - \hat{\theta}_2 \\ \tilde{b}_1 &= \hat{b}_1^* - \hat{b}_1,\ \ \tilde{b}_2 = \hat{b}_2^* - \hat{b}_2\end{aligned} \tag{27}$$

Considering the estimated dynamics of $\hat{y}_1$ and $\hat{y}_2$, u_p and u_b can be written as:

$$\begin{aligned}u_p &= \left(-\hat{f}_1\left(y,\theta_1\right) - \lambda_1e_1 + s_{p_c}\right)/\hat{b}_1 \\ u_b &= \left(-\hat{f}_2\left(y,\theta_2\right) - \lambda_2e_2 + s_{b_c}\right)/\hat{b}_2\end{aligned} \tag{28}$$

Considering (28) and (22), the dynamics of e_1 and e_2 can be written as:

$$\begin{aligned}\dot{e}_1 &= -\lambda_1e_1 + s_{p_c} \\ \dot{e}_2 &= -\lambda_2e_2 + s_{b_c}\end{aligned} \tag{29}$$

To stability analysis, consider a Lyapunov function as:

$$\begin{aligned}V &= \frac{1}{2}\tilde{y}_1^2 + \frac{1}{2}\tilde{y}_2^2 + \frac{1}{2}e_1^2 + \frac{1}{2}e_2^2 \\ &\quad + \frac{1}{2\gamma}\tilde{b}_1^2 + \frac{1}{2\gamma}\tilde{b}_2^2 + \frac{1}{2\gamma}\tilde{\theta}_1^T\tilde{\theta}_1 + \frac{1}{2\gamma}\tilde{\theta}_2^T\tilde{\theta}_2 \\ &\quad + \frac{1}{2\gamma}\tilde{\bar{E}}_1^2 + \frac{1}{2\gamma}\tilde{\bar{E}}_2^2\end{aligned} \tag{30}$$

where, $\tilde{\bar{E}}_i,\ i = 1,2$ are defined as:

$$\tilde{\bar{E}}_i = \bar{E}_i - \hat{\bar{E}}_i \tag{31}$$

where, $\bar{E}_i$ is the upper bound of AE E_i, and $\hat{\bar{E}}_i$ represents the estimation of $\bar{E}_i$. From (30), $\dot{V}$ becomes:

$$\begin{aligned}\dot{V} &= \dot{\tilde{y}}_1\tilde{y}_1 + \dot{\tilde{y}}_2\tilde{y}_2 + \dot{e}_1e_1 + \dot{e}_2e_2 \\ &\quad - \frac{1}{\gamma}\tilde{b}_1\dot{\hat{b}}_1 - \frac{1}{\gamma}\tilde{b}_2\dot{\hat{b}}_2 - \frac{1}{\gamma}\tilde{\theta}_1^T\dot{\hat{\theta}}_1 - \frac{1}{\gamma}\tilde{\theta}_2^T\dot{\hat{\theta}}_2 \\ &\quad - \frac{1}{\gamma}\tilde{\bar{E}}_1\dot{\hat{\bar{E}}}_1 + -\frac{1}{\gamma}\tilde{\bar{E}}_2\dot{\hat{\bar{E}}}_2\end{aligned} \tag{32}$$

From equations (29) and (26), $\dot{V}$ is rewritten as:

$$\begin{aligned}\dot{V} &= \tilde{y}_1\left(\tilde{\theta}_1^T\xi_1 + \tilde{b}_1u_p + E_1\right) + \tilde{y}_2\left(\tilde{\theta}_2^T\xi_2 + \tilde{b}_2u_b + E_2\right) \\ &\quad + e_1\left(-\lambda_1e_1 + s_{p_c}\right) + e_2\left(-\lambda_2e_2 + s_{b_c}\right) \\ &\quad - \frac{1}{\gamma}\tilde{\theta}_1^T\dot{\hat{\theta}}_1 - \frac{1}{\gamma}\tilde{\theta}_2^T\dot{\hat{\theta}}_2 - \frac{1}{\gamma}\tilde{b}_1\dot{\hat{b}}_1 - \frac{1}{\gamma}\tilde{b}_2\dot{\hat{b}}_2 \\ &\quad - \frac{1}{\gamma}\tilde{\bar{E}}_1\dot{\hat{\bar{E}}}_1 + -\frac{1}{\gamma}\tilde{\bar{E}}_2\dot{\hat{\bar{E}}}_2\end{aligned} \tag{33}$$

The equation (33) can be rewritten as:

$$\begin{aligned}\dot{V} &= s_{p_c}e_1 + s_{b_c}e_2 - \lambda_1e_1^2 - \lambda_2e_2^2 \\ &\quad + \tilde{\theta}_1^T\left(\tilde{y}_1\xi_1 - \frac{1}{\eta}\dot{\hat{\theta}}_1\right) + \tilde{\theta}_2^T\left(\tilde{y}_2\xi_2 - \frac{1}{\eta}\dot{\hat{\theta}}_2\right) \\ &\quad + \tilde{b}_1\left(\tilde{y}_1u_p - \frac{1}{\eta}\dot{\hat{b}}_1\right) + \tilde{b}_2\left(\tilde{y}_2u_b - \frac{1}{\eta}\dot{\hat{b}}_2\right) \\ &\quad + E_1\tilde{y}_1 + E_2\tilde{y}_2 - \frac{1}{\gamma}\tilde{\bar{E}}_1\dot{\hat{\bar{E}}}_1 + -\frac{1}{\gamma}\tilde{\bar{E}}_2\dot{\hat{\bar{E}}}_2\end{aligned} \tag{34}$$

From (19), $\dot{V}$ is rewritten as:

$$\begin{aligned}\dot{V} &= -\lambda_1e_1^2 - \lambda_2e_2^2 + s_{p_c}e_1 + s_{b_c}e_2 + E_1\tilde{y}_1 + E_2\tilde{y}_2 \\ &\quad - \frac{1}{\gamma}\tilde{\bar{E}}_1\dot{\hat{\bar{E}}}_1 + -\frac{1}{\gamma}\tilde{\bar{E}}_2\dot{\hat{\bar{E}}}_2\end{aligned} \tag{35}$$

From (31) and (35), $\dot{V}$, becomes:

$$\begin{aligned}\dot{V} &= -\lambda_1e_1^2 - \lambda_2e_2^2 + s_{p_c}e_1 + s_{b_c}e_2 + E_1\tilde{y}_1 + E_2\tilde{y}_2 \\ &\quad - \frac{1}{\gamma}\left(\bar{E}_1 - \hat{\bar{E}}_1\right)\dot{\hat{\bar{E}}}_1 + -\frac{1}{\gamma}\left(\bar{E}_2 - \hat{\bar{E}}_2\right)\dot{\hat{\bar{E}}}_2\end{aligned} \tag{36}$$

From (36), it is concluded that:

$$\begin{aligned}\dot{V} &\leq -\lambda_1e_1^2 - \lambda_2e_2^2 + s_{p_c}e_1 + s_{b_c}e_2 \\ &\quad + \bar{E}_1\left|\tilde{y}_1\right| + \bar{E}_2\left|\tilde{y}_2\right| \\ &\quad - \frac{1}{\gamma}\left(\bar{E}_1 - \hat{\bar{E}}_1\right)\dot{\hat{\bar{E}}}_1 + -\frac{1}{\gamma}\left(\bar{E}_2 - \hat{\bar{E}}_2\right)\dot{\hat{\bar{E}}}_2\end{aligned} \tag{37}$$

The inequality (37) can be simplified as:

$$\begin{aligned}\dot{V} &\leq -\lambda_1e_1^2 - \lambda_2e_2^2 + s_{p_c}e_1 + s_{b_c}e_2 \\ &\quad + \bar{E}_1\left(\left|\tilde{y}_1\right| - \frac{1}{\gamma}\dot{\hat{\bar{E}}}_1\right) + \bar{E}_2\left(\left|\tilde{y}_2\right| - \frac{1}{\gamma}\dot{\hat{\bar{E}}}_2\right) \\ &\quad + \frac{1}{\gamma}\hat{\bar{E}}_1\dot{\hat{\bar{E}}}_1 + \frac{1}{\gamma}\hat{\bar{E}}_2\dot{\hat{\bar{E}}}_2\end{aligned} \tag{38}$$

By substituting (20) into (38), one has:

$$\begin{aligned}\dot{V} &\leq -\lambda_1e_1^2 - \lambda_2e_2^2 + s_{p_c}e_1 + s_{b_c}e_2 \\ &\quad + \frac{1}{\gamma}\hat{\bar{E}}_1\dot{\hat{\bar{E}}}_1 + \frac{1}{\gamma}\hat{\bar{E}}_2\dot{\hat{\bar{E}}}_2\end{aligned} \tag{39}$$

Substituting s_{p_c} and s_{b_c} from (18), yields:

$$\dot{V} \leq -\lambda_1e_1^2 - \lambda_2e_2^2 +$$

$$-\hat{\hat{E}}_1\left|\tilde{y}_1\right|\frac{e_1^2}{\left|e_1^2\right|+\varepsilon}-\hat{\hat{E}}_2\left|\tilde{y}_2\right|\frac{e_2^2}{\left|e_2^2\right|+\varepsilon}$$
$$+\frac{1}{\gamma}\hat{\tilde{E}}_1\dot{\hat{\hat{E}}}_1+\frac{1}{\gamma}\hat{\tilde{E}}_2\dot{\hat{\hat{E}}}_2 \tag{40}$$

From (20) and (43), one has:

$$\begin{aligned}\dot{V} \leq & -\lambda_1 e_1^2-\lambda_2 e_2^2+\\ & -\hat{\hat{E}}_1\left|\tilde{y}_1\right|\frac{e_1^2}{\left|e_1^2\right|+\varepsilon}-\hat{\hat{E}}_2\left|\tilde{y}_2\right|\frac{e_2^2}{\left|e_2^2\right|+\varepsilon}\\ & +\hat{\hat{E}}_1\left|\tilde{y}_1\right|+\hat{\hat{E}}_2\left|\tilde{y}_2\right|\end{aligned} \tag{41}$$

The inequality (41) is simplified as:

$$\begin{aligned}\dot{V} \leq & -\lambda_1 e_1^2-\lambda_2 e_2^2\\ & -\hat{\hat{E}}_1\left|\tilde{y}_1\right|\left(\frac{e_1^2}{\left|e_1^2\right|+\varepsilon}-1\right)\\ & -\hat{\hat{E}}_2\left|\tilde{y}_2\right|\left(\frac{e_2^2}{\left|e_2^2\right|+\varepsilon}-1\right)\end{aligned} \tag{42}$$

From the fact that $e_1^2 \approx \left(\left|e_1^2\right|+\varepsilon\right)$ and $e_2^2 \approx \left(\left|e_2^2\right|+\varepsilon\right)$, one has:

$$\dot{V} \leq -\lambda_1 e_1^2-\lambda_2 e_2^2 \leq 0 \tag{43}$$

From (43), it is seen that $\dot{V} \leq 0$, when:

$$e_i=0, \tilde{y}_i \neq 0, \tilde{b}_i \neq 0, \tilde{\theta}_i \neq 0, \tilde{\hat{E}}_i \neq 0 \tag{44}$$

Since the objective of the control system is to derive $e_i=0$ and the invariant set of the closed-loop system do not include $\left(\tilde{y}_i, \tilde{b}_i, \tilde{\theta}_i, \tilde{\hat{E}}_i\right)$, then from La Salle's invariant set theorem the asymptotic stability is concluded. The proof is completed. □

Remark 2: The convergence speed of the suggested controller depends on the values of λ_1, λ_2 in (17) and estimation accuracy of IT3-FLSs.

Remark 3: Although the dynamics of units are considered to be unknown, however, to implement the suggested controller, it is need that the currents of PV and battery and output voltage to be measured, accurately. For the future studies, the possibility of removing the measurement of all states can be studied.

V. SIMULATION STUDIES

The performance of the suggested power management system is examined through simulations. The value of parameters of the considered models are given in Table 3. The other control parameters as: $\gamma=0.5$, $\varepsilon=0.1$, $\lambda_i=50$, $i=1,2$, $\bar{c}_{\tilde{A}_{I_b}}=4$, $\bar{c}_{\tilde{A}_{I_p}}=4$, $\underline{c}_{\tilde{A}_{I_b}}=0$, $\underline{c}_{\tilde{A}_{I_p}}=0$, $\bar{c}_{\tilde{A}_{V_c}}=24$, $\underline{c}_{\tilde{A}_{V_c}}=10$, $\bar{\sigma}_{\tilde{A}_{I_b}}=4$, $\bar{\sigma}_{\tilde{A}_{I_p}}=4$, $\underline{\sigma}_{\tilde{A}_{I_b}}=2$, $\underline{\sigma}_{\tilde{A}_{I_p}}=2$, $\bar{\sigma}_{\tilde{A}_{V_c}}=10$ and $\underline{\sigma}_{\tilde{A}_{V_c}}=5$.

Remark 4: The centers and the standard divisions of MFs for inputs of IT3-FLSs are determined on basis of input range, but the consequent parameters are online updated. The other parameters λ_i should be positive, ε is a small constant and $0<\gamma\leq 1$

A. SCENARIO 1

For 1-th scenario, the radiation is considered to be fixed at level 450 w/m^2. The trajectories of signals I_p, P, V_c are shown in Figs. 7-9 and controllers u_p/u_b are given in Figs. 10-11. One can observes that, a well tracking response is achieved and the control signals have good shape with no chattering.

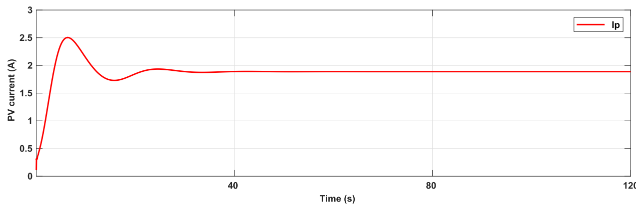

FIGURE 7. Scenario 1: Current of PV.

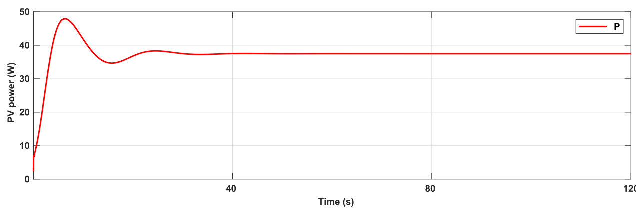

FIGURE 8. Scenario 1: Power of PV.

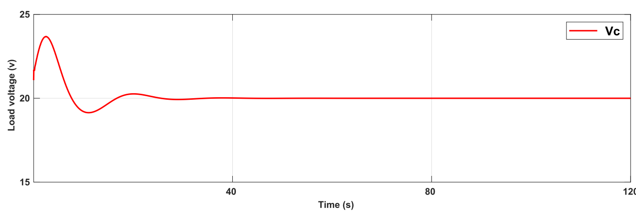

FIGURE 9. Scenario 1: Load voltage.

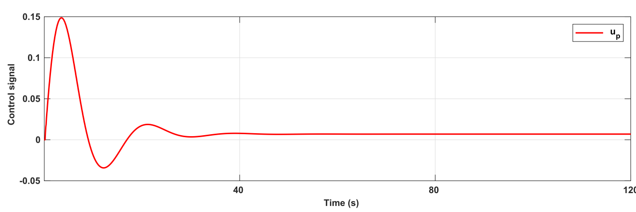

FIGURE 10. Scenario 1: u_p.

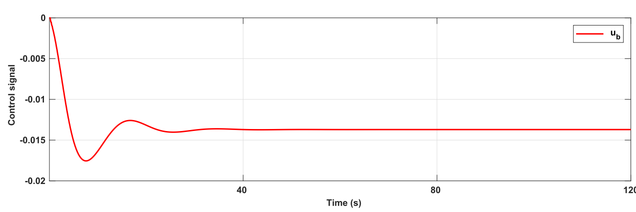

FIGURE 11. Scenario 1: u_b.

B. SCENARIO 2

In the second scenario the capability of the suggested scheme is examined under difficult condition. The temperature, load

TABLE 3. Simulation parameters.

Parameter	value	Parameter	value
L_p	4 (mH)	L_b	10 (mH)
P_b	55 (w)	i_{sc}	3.45 (A)
C	600 (μf)	r_p	30 $(m\Omega)$
T_r	$(^{\circ}C)$	k_i	1.2 (A/k)
A	1.2	V_{boc}	9 (v)
i_r	5.99e-8 (A)	E_g	1.12 (ev)
β_1	0.9	β_2	1.1
r_b	80 $(m\Omega)$	k_b	1.381e-23
P_b	21 (w)	W_{Loss}	20 (w)
q	1.60e-19	n	36

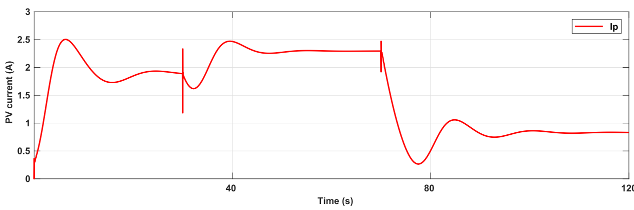

FIGURE 12. Scenario 2: Current of PV.

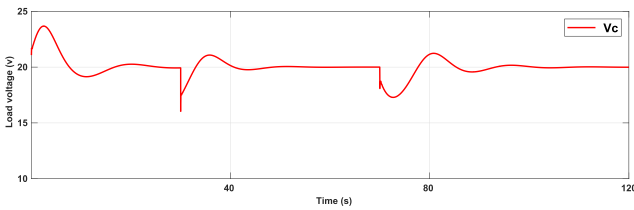

FIGURE 13. Scenario 2: Load voltage.

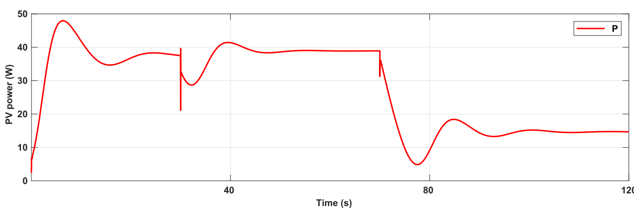

FIGURE 14. Scenario 2: Power of PV.

and radiation are considered to be time-varying such that, temperature is changed from 11 to 50 $(^{\circ}C)$ at time $t = 30$s, the load is varied from 75 into 35 (Ω) at time $t = 100$s and the irradiation is changed from 450 into 251 (w/m^2) at $t = 70$s. The trajectories of signals I_p, P, V_c are given in Figs. 12-13 and the signals u_p and u_b are shown in Figs. 15-16. From Figs. 12-13 one can see a well robustness performance against time-varying temperature, load and radiation. Also, a good output voltage regulation is achieved and the power of PV well tracks the changes of conditions.

Remark 5: The simulation are carried out by Matlab 2018a, i7-4720HQ CPU 2.60 GH. The simulation time is about 129s.

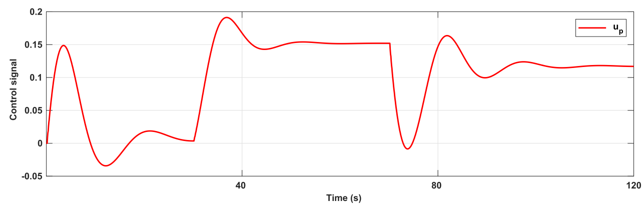

FIGURE 15. Scenario 2: Control signal u_p.

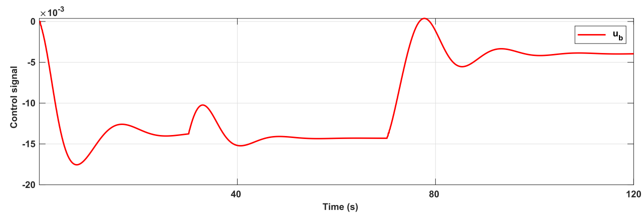

FIGURE 16. Scenario 2: Control signal u_b.

C. COMPARISON

To better show the capability of the proposed mechanism, a comparison with some other well-known regulators is provided such as PID controller [47], linear quadrature regulator (LQR) [48], passivity based regulator (PBR) [49], and sliding mode control scheme (SMC) [50]. The comparison results are given in Table 4 in term of mean square error (MSE). It is seen that the schemed controller results in better regulation performance. To further examination of the effectiveness of the suggested FLS based controller, another comparison is given by considering other type of FLS in the schemed controller. After 20 times repeating of simulation, the minimum (Min) and maximum (Max) of MSE are given in Table 5. The results in Table 5, clearly show the superiority of the proposed IT3-FLS.

Remark 6: The simulation results show that the designed control scheme performs desirably and the output voltage remain fixed under various perturbations such as variation of load and irradiation.

TABLE 4. MSE comparison considering various regulators.

Signal	Method				
	LQR [48]	PID [47]	PBR [49]	SMC [50]	Proposed controller
V_c	148.9197	15.2294	11.2499	9.3327	0.8724
I_p	0.8259	1.1029	0.9579	0.5161	0.3198

TABLE 5. MSE Comparison considering various fuzzy neural networks.

	FLSs					
	type-1		type-2		type-3	
Signal	Min of MSE	Max of MSE	Min of MSE	Max of MSE	Min of MSE	Max of MSE
V_c	1.8731	1.8732	1.1214	1.1216	0.8724	0.8725
I_p	0.9321	0.9321	0.6261	0.6262	0.3198	0.3199

VI. CONCLUSION

In this study a new approach has been presented for power management in PV/Battery systems. A new IT3-FLS has been designed to estimate the uncertain dynamics. The robustness and stability analysis have been done by taking an appropriate Lyapunov function and some tuning rules have been extracted for IT3-FLS and control signals. A new compensator has been proposed to cope with the effects of dynamic estimation error. In various scenarios the capability of the proposed method has been examined. For the first one, a normal condition has been considered and it has been shown that the current of PV, output voltage and power of PV are regulated in the desired levels. For second one, in addition to the variation of temperature and time-varying radiation, an abruptly changing in output load has been also considered. It has been observed that a well performance is achieved. For the last examination, to better show the superiority of proposed scheme, two comparisons with some other well known controllers and other FLS have been given. For the future studies, the effect of actuator failure on stability and the possibility of removing the measurement of all states can be considered.

REFERENCES

[1] A. Chakir, M. Tabaa, F. Moutaouakkil, H. Medromi, M. Julien-Salame, A. Dandache, and K. Alami, ''Optimal energy management for a grid connected PV-battery system,'' *Energy Rep.*, vol. 6, pp. 218–231, Feb. 2020.

[2] I. El Kafazi, M. Lafkih, and R. Bannari, ''PV generator and energy storage systems for laboratory building,'' *Energy Rep.*, vol. 6, pp. 672–679, Feb. 2020.

[3] Y. Guo, X. Dai, K. Jermsittiparsert, and N. Razmjooy, ''An optimal configuration for a battery and PEM fuel cell-based hybrid energy system using developed krill herd optimization algorithm for locomotive application,'' *Energy Rep.*, vol. 6, pp. 885–894, Nov. 2020.

[4] Y. Cao, H. Yao, Z. Wang, K. Jermsittiparsert, and N. Yousefi, ''Optimal designing and synthesis of a hybrid PV/fuel cell/wind system using metaheuristics,'' *Energy Rep.*, vol. 6, pp. 1353–1362, Nov. 2020.

[5] A. Awasthi, A. K. Shukla, M. M. S. R. C. Dondariya, K. N. Shukla, D. Porwal, and G. Richhariya, ''Review on sun tracking technology in solar PV system,'' *Energy Rep.*, vol. 6, pp. 392–405, Nov. 2020.

[6] J. Li and M. A. Danzer, ''Optimal charge control strategies for stationary photovoltaic battery systems,'' *J. Power Sources*, vol. 258, pp. 365–373, Jul. 2014.

[7] Z. Wu, H. Tazvinga, and X. Xia, ''Demand side management of photovoltaic-battery hybrid system,'' *Appl. Energy*, vol. 148, pp. 294–304, Jun. 2015.

[8] K. Wu, H. Zhou, S. An, and T. Huang, ''Optimal coordinate operation control for wind–photovoltaic–battery storage power-generation units,'' *Energy Convers. Manage.*, vol. 90, pp. 466–475, Jan. 2015.

[9] M. R. Mojallizadeh and M. A. Badamchizadeh, ''Adaptive passivity-based control of a Photovoltaic/Battery hybrid power source via algebraic parameter identification,'' *IEEE J. Photovolt.*, vol. 6, no. 2, pp. 532–539, Mar. 2016.

[10] Y. Guan, J. C. Vasquez, J. M. Guerrero, Y. Wang, and W. Feng, ''Frequency stability of hierarchically controlled hybrid Photovoltaic-Battery-Hydropower microgrids,'' *IEEE Trans. Ind. Appl.*, vol. 51, no. 6, pp. 4729–4742, Nov. 2015.

[11] J. R. Prabhakar and K. Ragavan, ''Power management based current control technique for photovoltaic-battery assisted wind–hydro hybrid system,'' *Int. J. Emerg. Electr. Power Syst.*, vol. 14, no. 4, pp. 351–362, 2013.

[12] T. Shimada and K. Kurokawa, ''Grid-connected photovoltaic systems with battery storages control based on insolation forecasting using weather forecast,'' *Renew. Energy*, pp. 228–230, 2006.

[13] F. Zaouche, D. Rekioua, J.-P. Gaubert, and Z. Mokrani, ''Supervision and control strategy for photovoltaic generators with battery storage,'' *Int. J. Hydrogen Energy*, vol. 42, no. 30, p. 19 536–19 555, 2017.

[14] P. P. Mishra, M. Denlinger, and H. K. Fathy, ''Estimation-based maximum power point tracking in a self-balancing photovoltaic battery energy storage system,'' *J. Dyn. Syst., Meas., Control*, vol. 141, no. 10, Oct. 2019.

[15] R. Zhang and B. Hredzak, ''Nonlinear sliding mode and distributed control of battery energy storage and photovoltaic systems in AC microgrids with communication delays,'' *IEEE Trans. Ind. Informat.*, vol. 15, no. 9, pp. 5149–5160, Sep. 2019.

[16] Y. Cao, Q. Wang, W. Cheng, S. Nojavan, and K. Jermsittiparsert, ''Risk-constrained optimal operation of fuel cell/photovoltaic/battery/grid hybrid energy system using downside risk constraints method,'' *Int. J. Hydrogen Energy*, vol. 45, no. 27, pp. 14108–14118, May 2020.

[17] M. Errouha, A. Derouich, S. Motahhir, O. Zamzoum, N. El Ouanjli, and A. El Ghzizal, ''Optimization and control of water pumping PV systems using fuzzy logic controller,'' *Energy Rep.*, vol. 5, pp. 853–865, Nov. 2019.

[18] R. Rathi, C. Prakash, S. Singh, G. Krolczyk, and C. I. Pruncu, ''Measurement and analysis of wind energy potential using fuzzy based hybrid MADM approach,'' *Energy Rep.*, vol. 6, pp. 228–237, Nov. 2020.

[19] M. H. Parvaneh and P. G. Khorasani, ''A new hybrid method based on fuzzy logic for maximum power point tracking of photovoltaic systems,'' *Energy Rep.*, vol. 6, pp. 1619–1632, Nov. 2020.

[20] K. Mansiri, S. Sukchai, and C. Sirisamphanwong, ''Fuzzy control for smart PV-battery system management to stabilize grid voltage of 22 kV distribution system in thailand,'' *Energies*, vol. 11, no. 7, p. 1730, Jul. 2018.

[21] Y. Liu and W. Kang, ''Fuzzy control based energy management strategy for microgrid system with photovoltaic and energy storage,'' in *Proc. CSU-EPSA*, 2017, vol. 1, no. 29, pp. 97–102.

[22] M. S. S. Amirhosein Mosavi, S. N. Qasem, and A. Mohammadzadeh, ''Fractional-order fuzzy control approach for photovoltaic/battery systems under unknown dynamics, variable irradiation and temperature,'' *Electronics*, vol. 9, p. 1455, Sep. 2020, doi: 10.3390/electronics9091455.
[23] Z. Roumila, D. Rekioua, and T. Rekioua, ''Energy management based fuzzy logic controller of hybrid system wind/photovoltaic/diesel with storage battery,'' *Int. J. Hydrogen Energy*, vol. 42, no. 30, pp. 19525–19535, 2017.
[24] S. Faquir, A. Yahyaouy, H. Tairi, and J. Sabor, ''Energy management in a hybrid pv/wind/battery system using a type-1 fuzzy logic computer algorithm,'' *Int. J. Intell. Eng. Inform.*, vol. 4, nos. 3–4, pp. 229–244, 2016.
[25] W. Mao, N. Dai, and H. Li, ''Economic dispatch of microgrid considering fuzzy control based storage battery charging and discharging,'' *J. Electr. Syst.*, vol. 15, no. 3, pp. 417–428, 2019.
[26] Y. Zou, F. Yan, X. Wang, and J. Zhang, ''An efficient fuzzy logic control algorithm for photovoltaic maximum power point tracking under partial shading condition,'' *J. Franklin Inst.*, vol. 357, no. 6, pp. 3135–3149, Apr. 2020.
[27] X. Li and H. Yan, ''Fuzzy logic-based coordinated control method for multi-type battery energy storage systems,'' *Artif. Intell. Rev.*, vol. 49, no. 2, pp. 227–243, Feb. 2018.
[28] Kim, Huh, and Ko, ''Improvement of MPPT control performance using fuzzy control and VGPI in the PV system for micro grid,'' *Sustainability*, vol. 11, no. 21, p. 5891, Oct. 2019.
[29] Y. Wang, C. K. Ahn, H. Yan, and S. Xie, ''Fuzzy control and filtering for nonlinear singularly perturbed Markov jump systems,'' *IEEE Trans. Cybern.*, vol. 51, no. 1, pp. 297–308, Jan. 2021.
[30] Y. Wang, X. Xie, M. Chadli, S. Xie, and Y. Peng, ''Sliding mode control of fuzzy singularly perturbed descriptor systems,'' *IEEE Trans. Fuzzy Syst.*, early access, May 29, 2020, doi: 10.1109/TFUZZ.2020.2998519.
[31] H. Liang, G. Liu, H. Zhang, and T. Huang, ''Neural-network-based event-triggered adaptive control of nonaffine nonlinear multiagent systems with dynamic uncertainties,'' *IEEE Trans. Neural Netw. Learn. Syst.*, early access, Jul. 14, 2020, doi: 10.1109/TNNLS.2020.3003950.
[32] H. Zhang, Y. Liu, J. Dai, and Y. Wang, ''Command filter based adaptive fuzzy finite-time control for a class of uncertain nonlinear systems with hysteresis,'' *IEEE Trans. Fuzzy Syst.*, early access, Jun. 18, 2020, doi: 10.1109/TFUZZ.2020.3003499.
[33] H. Zhang, Y. Liu, and Y. Wang, ''Observer-based finite-time adaptive fuzzy control for nontriangular nonlinear systems with full-state constraints,'' *IEEE Trans. Cybern.*, early access, Apr. 29, 2020, doi: 10.1109/TCYB.2020.2984791.
[34] H. Liang, X. Guo, Y. Pan, and T. Huang, ''Event-triggered fuzzy bipartite tracking control for network systems based on distributed reduced-order observers(revised manuscript of TFS-2019-1049),'' *IEEE Trans. Fuzzy Syst.*, early access, Mar. 23, 2020, doi: 10.1109/TFUZZ.2020.2982618.
[35] P. S. Kumar, ''PSK method for solving type-1 and type-3 fuzzy transportation problems,'' *Int. J. Fuzzy Syst. Appl.*, vol. 5, no. 4, pp. 121–146, Oct. 2016.
[36] N. Nabipour, S. N. Qasem, and K. Jermsittiparsert, ''Type-3 fuzzy voltage management in pv/hydrogen fuel cell/battery hybrid systems,'' *Int. J. Hydrogen Energy*, vol. 45, no. 56, pp. 32478–32492, 2020.
[37] A. Mohammadzadeh, M. H. Sabzalian, and W. Zhang, ''An interval type-3 fuzzy system and a new online fractional-order learning algorithm: Theory and practice,'' *IEEE Trans. Fuzzy Syst.*, vol. 28, no. 9, pp. 1940–1950, Sep. 2020.
[38] P. Bhowmik, S. Chandak, and P. K. Rout, ''State of charge and state of power management among the energy storage systems by the fuzzy tuned dynamic exponent and the dynamic PI controller,'' *J. Energy Storage*, vol. 19, pp. 348–363, Oct. 2018.
[39] H. Hassani, J. Zarei, M. M. Arefi, and R. Razavi-Far, ''zSlices-based general type-2 fuzzy fusion of support vector machines with application to bearing fault detection,'' *IEEE Trans. Ind. Electron.*, vol. 64, no. 9, pp. 7210–7217, Sep. 2017.
[40] J. Andreu-Perez, F. Cao, H. Hagras, and G.-Z. Yang, ''A self-adaptive online brain–machine interface of a humanoid robot through a general type-2 fuzzy inference system,'' *IEEE Trans. Fuzzy Syst.*, vol. 26, no. 1, pp. 101–116, Feb. 2018.
[41] E. Ontiveros, P. Melin, and O. Castillo, ''Comparative study of interval type-2 and general type-2 fuzzy systems in medical diagnosis,'' *Inf. Sci.*, vol. 525, pp. 37–53, Jul. 2020.
[42] H. A. Al-Jamimi and T. A. Saleh, ''Transparent predictive modelling of catalytic hydrodesulfurization using an interval type-2 fuzzy logic,'' *J. Cleaner Prod.*, vol. 231, pp. 1079–1088, Sep. 2019.
[43] E. Ontiveros-Robles and P. Melin, ''Toward a development of general type-2 fuzzy classifiers applied in diagnosis problems through embedded type-1 fuzzy classifiers,'' *Soft Comput.*, vol. 24, no. 1, pp. 83–99, Jan. 2020.
[44] G. E. Martínez, C. I. Gonzalez, O. Mendoza, and P. Melin, ''General type-2 fuzzy Sugeno integral for edge detection,'' *J. Imag.*, vol. 5, no. 8, p. 71, Aug. 2019.
[45] Y. Wu, T. Zhang, and L. Yi, ''An internal type-2 trapezoidal fuzzy Sets-PROMETHEE-II based investment decision framework of compressed air energy storage project in China under the perspective of different investors,'' *J. Energy Storage*, vol. 30, Aug. 2020, Art. no. 101548.
[46] B. Lin, ''Conceptual design and modeling of a fuel cell scooter for urban Asia,'' *J. Power Sources*, vol. 86, nos. 1–2, pp. 202–213, Mar. 2000.
[47] S. W. Sung, J. Lee, and I.-B. Lee, *Process Identification PID Control*, vol. 6. Hoboken, NJ, USA: Wiley, 2009.
[48] D. E. Kirk, *Optimal Control Theory: Introduction*. North Chelmsford, MA, USA: Courier Corporation, 2012.
[49] A. Tofighi and M. Kalantar, ''Power management of PV/battery hybrid power source via passivity-based control,'' *Renew. Energy*, vol. 36, no. 9, pp. 2440–2450, Sep. 2011.
[50] M. R. Mojallizadeh, M. Badamchizadeh, S. Khanmohammadi, and M. Sabahi, ''Designing a new robust sliding mode controller for maximum power point tracking of photovoltaic cells,'' *Sol. Energy*, vol. 132, pp. 538–546, Jul. 2016.